arXiv:cond-mat/0308232v1 [cond-mat.mtrl-sci] 12 Aug 2003

ELECTROMECHANICAL PROPERTIES OF MULTI-DOMAIN FERROELECTRICS

Rajeev Ahluwalia,[1] Turab Lookman,[1] Avadh Saxena,[1] and Wenwu Cao[2]

[1]*Theoretical Division, Los Alamos National Laboratory, Los Alamos, New Mexico, 87545*
[2]*Materials Research Institute and Department of Mathematics, Pennsylvania State University, Pennsylvania 16802*

(Dated: February 2, 2008)

We study theoretically the influence of the underlying domain microstructure on the electromechanical properties of ferroelectrics. Our calculations are based on a continuum approach that incorporates the long-range elastic and electrostatic interactions. The theory is used to simulate the piezoelectric properties of a two dimensional model ferroelectric crystal. Simulation results indicate that the electromechanical response of the ferroelectric is strongly dependent on the domain microsctructure, including domain walls. This is particularly true for the case when an electric field is applied along a non-polar direction.

PACS numbers: 77.65.-j, 74.20.De, 77.65.Ly, 77.80.-e

Ferroelectrics are the best piezoelectric materials that can convert electrical energy into mechanical energy and vice versa[1]. This electromechanical property arises due to the coupling of the spontaneous polarization with lattice strain. Many devices such as ultrasonic transducers and piezoelectric actuators make use of this property[2]. Recently, there has been considerable interest in this field due to the observation of a giant piezoelectric response when the applied field is along a non-polar direction[3,4]. It is believed that this "superpiezoelectric" response is due to the symmetry change caused by a rotation of the polarization towards the direction of the applied field[5]. Domain configurations produced by the non-polar direction field are termed *engineered domains*. There are also a large number of domain walls between the degenerate variants which affect the piezoelectric property. It is important to understand the role played by such domain microstructures on the piezoelectric response.

Electromechanical properties of ferroelectrics have been studied theoretically using first-principle calculations[5,6,7]. A continuum Landau theory describing a single domain or homogeneous state has been used to study the electromechanical properties of $BaTiO_3$ as function of temperature and electric field direction[8]. Although such calculations provide valuable insights into the physics of the polarization-strain coupling, they do not describe inhomogeneities due to domains and domain walls. In this Letter, we study the behavior of domain patterns under applied electric field and investigate how the microstructural evolution influences the average electromechanical response of ferroelectric materials.

Our approach is to use a time-dependent Ginzburg-Landau model[9,10] with long-range elastic and electrostatic effects. We restrict ourselves to a $2D$ ferroelectric transition to illustrate the basic principles and use parameters from a model for $BaTiO_3$ in our calculations[8]. We find that the electromechanical response is highly orientation and microstructure dependent. When the field is applied along one of the polar directions, domain switching results in higher strains compared to the single domain state. For fields applied along a non-polar direction, the domain walls serve as nucleation sites for a field induced structural phase transition.

The free-energy functional for a $2D$ ferroelectric system is written as $F = F_l + F_{em} + F_{es}$. Here F_l is the local free energy[8] that describes the ferroelectric transformation and is given as

$$\begin{aligned} F_l &= \int d\vec{r}\Big\{\alpha_1({P_x}^2+{P_y}^2)+\alpha_{11}({P_x}^4+{P_y}^4) \\ &+ \alpha_{12}{P_x}^2{P_y}^2+\alpha_{111}({P_x}^6+{P_y}^6) \\ &+ \alpha_{112}({P_x}^2{P_y}^4+{P_x}^4{P_y}^2)-E_xP_x-E_yP_y \\ &+ \frac{g_1}{2}({P_{x,x}}^2+{P_{y,y}}^2)+\frac{g_2}{2}({P_{x,y}}^2+{P_{y,x}}^2) \\ &+ g_3P_{x,x}P_{y,y}\Big\}, \end{aligned} \tag{1}$$

where P_x and P_y are the polarization components. The free energy coefficients $\alpha_1, \alpha_{11}, ..., \alpha_{112}$ determine the ferroelectric phase and the gradient coefficients g_1, g_2 and g_3 are a measure of domain wall energies. E_x and E_y are the components of an external electric field. Elastic properties are studied by using the strains $\eta_1 = \eta_{xx} + \eta_{yy}$, $\eta_2 = \eta_{xx} - \eta_{yy}$ and $\eta_3 = \eta_{xy}$, where η_{ij} is the linearized strain tensor defined as $\eta_{ij} = (u_{i,j} + u_{j,i})/2$ $(i, j = x, y)$, u_i being the components of the displacement vector. The electromechanical coupling is described in terms of these strain variables as the free energy $F_{em} = \lambda \int d\vec{r}[\{\eta_1 - Q_1({P_x}^2 + {P_y}^2)\}^2 + \{\eta_2 - Q_2({P_x}^2 - {P_y}^2)\}^2 + \{\eta_3 - Q_3P_xP_y\}^2]$. Here Q_1, Q_2 and Q_3 are obtained from the electrostrictive constants of the material as $Q_1 = Q_{11} + Q_{12}$, $Q_2 = Q_{11} - Q_{12}$ and $Q_3 = Q_{44}$ (electrostrictive constants describe coupling between strains and polarization as $\eta_{xx} = Q_{11}{P_x}^2 + Q_{12}{P_y}^2$, $\eta_{yy} = Q_{11}{P_y}^2 + Q_{12}{P_x}^2$ and $\eta_{xy} = Q_{44}P_xP_y$). Notice that the free energy F_{em} vanishes for a homogeneous state as the homogeneous strains in equilibrium are given by ${\eta_1}^e = Q_1({P_x}^2 + {P_y}^2)$, ${\eta_2}^e = Q_2({P_x}^2 - {P_y}^2)$, and ${\eta_3}^e = Q_3P_xP_y$. However, this free energy does not vanish for an inhomogeneous state. For an inhomogeneous state, the strains η_1, η_2 and η_3 are related to each other by the elastic compatibility constraint[11] $\nabla^2\eta_1 - (\frac{\partial^2}{\partial x^2} - \frac{\partial^2}{\partial y^2})\eta_2 - \frac{\partial^2}{\partial x \partial y}\eta_3 = 0$. Using this relation, the strain η_1 can be eliminated from F_{em} resulting in a nonlocal interaction between the strains involving η_2 and η_3. Using the equilibrium strains defined by ${\eta_2}^e$ and ${\eta_3}^e$, the electromechanical free energy can be written as

$$F_{em} = \lambda \int d\vec{k}|C_2(\vec{k})\Gamma_2(\vec{k}) + C_3(\vec{k})\Gamma_3(\vec{k}) - \Gamma_1(\vec{k})|^2, \tag{2}$$

where the $\vec{k} = 0$ mode has been excluded from the above integral. The constant λ is the strength of this nonlocal interaction and hence it influences the underlying microstructure. The quantities $\Gamma_1(\vec{k})$, $\Gamma_2(\vec{k})$ and $\Gamma_3(\vec{k})$ are respectively the Fourier transforms of $Q_1({P_x}^2 + {P_y}^2)$, $Q_2({P_x}^2 - {P_y}^2)$ and $Q_3 P_x P_y$, $C_2 = ({k_x}^2 - {k_y}^2)/({k_x}^2 + {k_y}^2)$ and $C_3 = k_x k_y/({k_x}^2 + {k_y}^2)$ are the orientation dependent kernels. The electrostatic contribution to the free energy is calculated by considering the depolarization energy[12] $F_{es} = -\mu \int d\vec{r}\{\vec{E_d} \cdot \vec{P} + \epsilon_0(\vec{E_d} \cdot \vec{E_d}/2)\}$, where $\vec{E_d}$ is the internal depolarization field due to the dipoles and μ is the strength of this interaction. The field $\vec{E_d}$ can be calculated from an underlying potential as $\vec{E_d} = -\vec{\nabla}\phi$. If we assume that there is no free charge in the system, then $\vec{\nabla} \cdot \vec{D} = 0$, where $\vec{D}$ is the electric displacement vector defined by $\vec{D} = \epsilon_0 \vec{E_d} + \vec{P}$. This equation gives rise to the constraint $-\epsilon_0 \nabla^2 \phi + \vec{\nabla} \cdot \vec{P} = 0$. The potential ϕ is eliminated from the free energy F_{es} using the above constraint to express F_{es} in Fourier space as

$$F_{es} = (\mu/2\epsilon_0) \int d\vec{k} |\hat{k_x} P_x(\vec{k}) + \hat{k_y} P_y(\vec{k})|^2. \qquad (3)$$

The above integral excludes the homogeneous $\vec{k} = 0$ mode which means that the homogeneous depolarization field due to surface charges has been neglected. The total energy is defined as $F = F_l + F_{em} + F_{es}$ with two additional constants, i.e. λ and μ are essential for the description of multi-domain states.

The dynamics of the polarization fields is given by the relaxational time-dependent Ginzburg-Landau equations $\frac{\partial P_i}{\partial t} = -\gamma \frac{\delta F}{\delta P_i}$, where γ is a dissipation coefficient and $i = x, y$ represents the polarization components. We first introduce rescaled variables defined as $u = P_x/P_0$, $v = P_y/P_0$, $\vec{\zeta} = \vec{r}/\delta$ and $t^* = \gamma|\alpha_1(T_0)|t$, where T_0 is a fixed temperature. In this work, we use the parameters[8] for $BaTiO_3$ for the local part of the free energy F_l. The parameters which can be dependent on the temperature T are: $\alpha_1 = 3.34 \times 10^5 (T - 381)$ VmC^{-1}, $\alpha_{11} = 4.69 \times 10^6 (T - 393) - 2.02 \times 10^8$ Vm^{5}C^{-3}, $\alpha_{111} = -5.52 \times 10^7 (T - 393) + 2.76 \times 10^9$ Vm^{9}C^{-5}, $\alpha_{12} = 3.23 \times 10^8$ Vm^{5}C^{-3} and $\alpha_{112} = 4.47 \times 10^9$ Vm^{9}C^{-5}. The electrostrictive constants are given as $Q_{11} = 0.11$ m^{4}C^{-2}, $Q_{12} = -0.045$ m^{4}C^{-2} and $Q_{44} = 0.029$ m^{4}C^{-2}. We assume that the coefficients $g_1 = g_2 = g_3 = g$ and use the value $g = 0.025 \times 10^{-7}$ Vm^3/C quoted in the literature[13]. To calculate the rescaled quantities, we use $T_0 = 298K$ and $P_0 = 0.26$ Cm^{-2} and $\delta \sim 6.7$ nm. The values chosen for the long-range parameters are $\lambda = 0.25|\alpha_1(T_0)|/{P_0}^2$ and $\mu = 20\epsilon_0|\alpha_1(T_0)|$.

The time-dependent Ginzburg-Landau model with the above rescaled parameters is used to simulate the domain patterns and electromechanical properties. The equations are discretized on a 128×128 grid with the Euler scheme using periodic boundary conditions. For the length rescaling factor $\delta \sim 6.7$ nm, this discretization corresponds to a system of size ~ 0.85 μm $\times 0.85$ μm. We first simulate the properties of this $2D$ model at $T = 298K$. At this temperature, the minima of the free energy F_l define a rectangular ferroelectric phase with the four degenerate states $(\pm 0.26, 0)$ Cm^{-2} and $(0, \pm 0.26)$ Cm^{-2}. The dynamical equations are solved starting from small amplitude random initial conditions corresponding to a quenched paraelectric phase. Domains of the four degenerate states form and a domain growth process takes place. Eventually, the growth stops and a stable multi-domain state shown in Fig. 1(a) is obtained. All four polarization variants exist in this state. Note that there are only 90^o walls (domain walls across which the polarization angle changes by ninety degree) and these walls are aligned along the [11] or $[\bar{1}1]$ directions. The domain wall orientations are governed by the underlyling symmetry encoded in the anisotropic kernel in F_{es}. Another interesting feature of this domain structure is that there is no charge accumulation. This is clear from the fact that there are no head-head or tail-tail configurations at the domain walls. At some of the domain junctions polarization vortices are observed and at other junctions the heads coming in appear to balance the tails going out, thereby maintaining zero net charge.

To simulate the effect of an external electric field, the evolution equations are solved with a varying E_y (electric field in the $[01]$ direction) while E_x is kept at zero. The domain configuration of Fig. 1(a) is the initial condition as E_y is varied quasi-statically (the system is allowed to relax for $t^* = 1000$ after each change) from $E_y = 0$ to $E_y = 72.07$ kV/cm in steps of 1.85 kV/cm. It is clear from figures 1(b)-1(d) that this electric field causes the unfavorable domains to switch and since the field is along one of the polarization directions, eventually ($E_y \sim 9$ kV/cm) a single domain polarized along the $[01]$ direction is established. On removing the field, the system stays in this single domain state and there is an underlying hysteresis. Figure 2(a) shows the variation of $\langle P_x \rangle$ and $\langle P_x \rangle$ with E_y for the situation shown in Fig. 1. Also shown is the effect of electric field E_y on P_x and P_y for an initial single domain with $P_x = 0$ and $P_y = 0.26$ Cm^{-2} (these single domain response curves are obtained by minimizing the homogeneous local free energy F_l only). Beyond $E_y \sim 9$ kV/cm, the single and multi-domain responses coincide as both correspond to single domain states.

The appearance of $\langle P_x \rangle$ during the transient indicates that the polarization reversal of the $P_y < 0$ regions is via rotation of dipoles instead of direct 180^o flipping. Because the simulation size is limited, the number of clockwise and counterclockwise rotating dipoles is different, so that a transient $\langle P_x \rangle$ is observed. This can only be observed in very small systems in reality. To study the electromechanical behavior, we have also computed the behavior of uniaxial strain with the applied electric field. The uniaxial strain is calculated as $\langle \eta_{yy}(E_y) \rangle - \langle \eta_{yy}(0) \rangle$, where $\eta_{yy} = Q_{11}{P_y}^2 + Q_{12}{P_x}^2$. Figure 2(b) shows the variation of the uniaxial strain with the electric field. The electromechanical response of the single domain state is also shown. It is clear that the multi-domain state generates much higher strain compared to the single domain case. The switching of 90^o domains provides the extra strain in the multi-domain state. The piezoelectric constant d_{33} (calculated as the slope of the strain vs. electric field curve) for the large field fully polarized state is nearly the same for both the single-domain and multi-domain responses (~ 82 pC/N). We have also calculated the dielectric

constant $\epsilon_{yy} = 1 + {\epsilon_0}^{-1}(dP_y/dE_y)$ for the saturated state from the P_y vs. E_y curve. The calculated dielectric constants are also nearly the same for both single- and multi-domain states ($\epsilon_{yy} \sim 150$) . Our findings are qualitatively in agreement with the experimental results of Wada et al.[4] and Park et al.[14] who have measured the electromechanical response of $BaTiO_3$ multi-domain single crystals at room temperature. For a quantitative comparison, a full $3D$ calculation is required. Nevertheless, our $2D$ calculation captures the essential physics of these experiments.

Next, we study the case with $T = 273K$. At this temperature, the free energy in F_l has four minima $(\pm 0.21, \pm 0.21)$ Cm^{-2} and $(\pm 0.21, \mp 0.21)$ Cm^{-2}, each state corresponding to a rhombic phase. As in the earlier case, growth of domains from the paraelectric phase results in a multi-domain state with all four variants, as shown in Fig. 3(a). However, for this case, the domain walls are oriented along [10] or [01] as dictated by the symmetry of the rhombic phase encoded in the anisotropic long-range interaction F_{es}. There is no net charge, even for this case. Here also, we apply the electric field along the $[01]$ direction. This situation is interesting as the $[01]$ direction is not one of the polarization directions at this temperature. Because of its superior piezoelectric properties, this situation has been studied in numerous experimental systems[3,4,14]. We vary the electric field E_y at the same rate as in the $T = 298K$ case. Unlike the earlier case, application of the field does not result in transformation to a single domain state. Instead, a stable multi-domain state that has only two of the variants $(P_y > 0)$ is formed at $E_y = 5.54$ kV/cm (Fig. 3b). This configuration is analogous to the *engineered domains* observed in recent experiments[3,4,14]. This engineered configuration persists till $E_y \sim 51kV/cm$, although individual polarization vectors gradually rotate towards the [01] direction. Figure 3(c) shows the domain pattern at $E_y = 51.74$ kV/cm. Here we can clearly see that polarization vectors have rotated and at the domain wall, the polarization is almost aligned with the [01] direction. Thus, the domain boundaries serve as a nucleation source for an electric field induced structural transition from a rhombic to a rectangular ferroelectric phase. The transition is complete at $E_y = 53.59$ kV/cm, as is clear from Fig. 3(d) where all the polarization vectors are aligned along the [01] direction. If we remove the field, the situation shown in Fig. 3(d) remains in a single domain rectangular state. However, if we remove the field before the field induced transition, the engineered configuration remains stable.

In Fig. 4(a), we show the variation of $\langle P_x \rangle$ and $\langle P_y \rangle$ for the situation depicted in Fig. 3. The appropriate single domain behavior starting from a polarized state $P_x = 0.21$ Cm^{-2} and $P_y = 0.21$ Cm^{-2} is also shown. Polarization rotation and field induced transition at $E_y \sim 53$ kV/cm for the multi-domain state is apparent from this figure. Interestingly, the transition occurs at a higher field value $E_y \sim 69$ kV/cm for the single domain state. This is due to the fact that in the single domain state, there are no nucleation mechanisms. Nucleation sources exist in the multi-domain state due to the domain walls. In the single domain calculations of Bell[8], the field induced transitions occured at much higher values than the experimental values. The present calculation suggests that domain walls can help to reduce the field level, similar to the effect of dipolar defects in reducing the coercive field during switching[10]. Figure 4(b) shows the electromechanical response for this situation for both single and multi-domain states. These curves are similar to the strain vs. electric field curves for experiments where the field is applied along non-polar directions[3,4,14]. In the domain engineered regime (before the field induced transition), high values of d_{33} due to polarization rotations are found. For example, the multi-domain $d_{33} \sim 567$ pC/N and the corresonding single domain $d_{33} \sim 367$ pC/N at $E_y = 49.89$ kV/cm are achieved. The corresponding dielectric constants are $\epsilon_{yy} \sim 750$ (multi-domain) and $\epsilon_{yy} \sim 525$ (single domain). The difference between the single domain and multi-domain electromechanical response shows the property enhancement due to the presence of domain walls.

To conclude, we have used a Ginzburg-Landau formalism to demonstrate the effect of the underlying domain microstructure on electromechanical properties of ferroelectrics. To account for nonlocal elastic and electrostatic effects, two additional parameters that measure the strength of the long-range interactions have been introduced. Our calculations show that these long-range parameters are essential to describe multi-domain states. In the present work, we have made simple choices for these parameters. In principle, these parameters should be measured for a given experimental multi-domain state for a complete characterization of the material.

[1] M. E Lines and A. M. Glass, *Principles and applications of ferroelectrics and related materials* (Clarendon, Oxford, 1979).

[2] K. Uchino, *Piezoelectric actuators and ultrasonic motors*, (Kluwer Academic, Boston, 1996).

[3] S. E. Park and T. R. Shrout, J. Appl. Phys. **82**, 1804 (1997).

[4] S. Wada, S. Suzuki, T. Noma, T. Suzuki, M. Osada, M. Kakihana, S. E. Park, L. E. Cross, and T R. Shrout, Jpn. J. Appl. Phys. **38**, 5505 (1999).

[5] H. Fu and R. E. Cohen, Nature (London) **403**, 281 (2000).

[6] A. Garcia and D. Vanderbilt, Appl. Phys. Lett. **72**, 2981 (1998).

[7] N. Sai, K. M. Rabe, and D. Vanderbilt, Phys. Rev. B **66**, 104108 (2002).

[8] A. J . Bell, J. Appl. Phys. **89**, 3907 (2001).

[9] S. Nambu and D. A. Sagala, Phys. Rev. B **50**, 5838 (1994).

[10] R. Ahluwalia and W.W. Cao, Phys. Rev B. **63**, 012103 (2001);

[11] E. A. H. Love, *A Treatise on the Mathematical Theory of Elasticity* (Dover, New York, 1944).

[12] A. M. Bratkovsky and A. P. Levanyuk, in *Fundamental Physics of Ferroelectrics*, ed. R. E. Cohen, AIP Conf. Proc. **626**, 252 (2002).

[13] T. Mitsui, I. Tatsuzaki and E. Nakamira, *An Introduction to the Physics of Ferroelectrics* (Gordon and Breach, New York, 1974).

[14] S. E. Park, S. Wada, L. E. Cross, and T. R. Shrout, J. Appl. Phys. **86**, 2746 (1999).

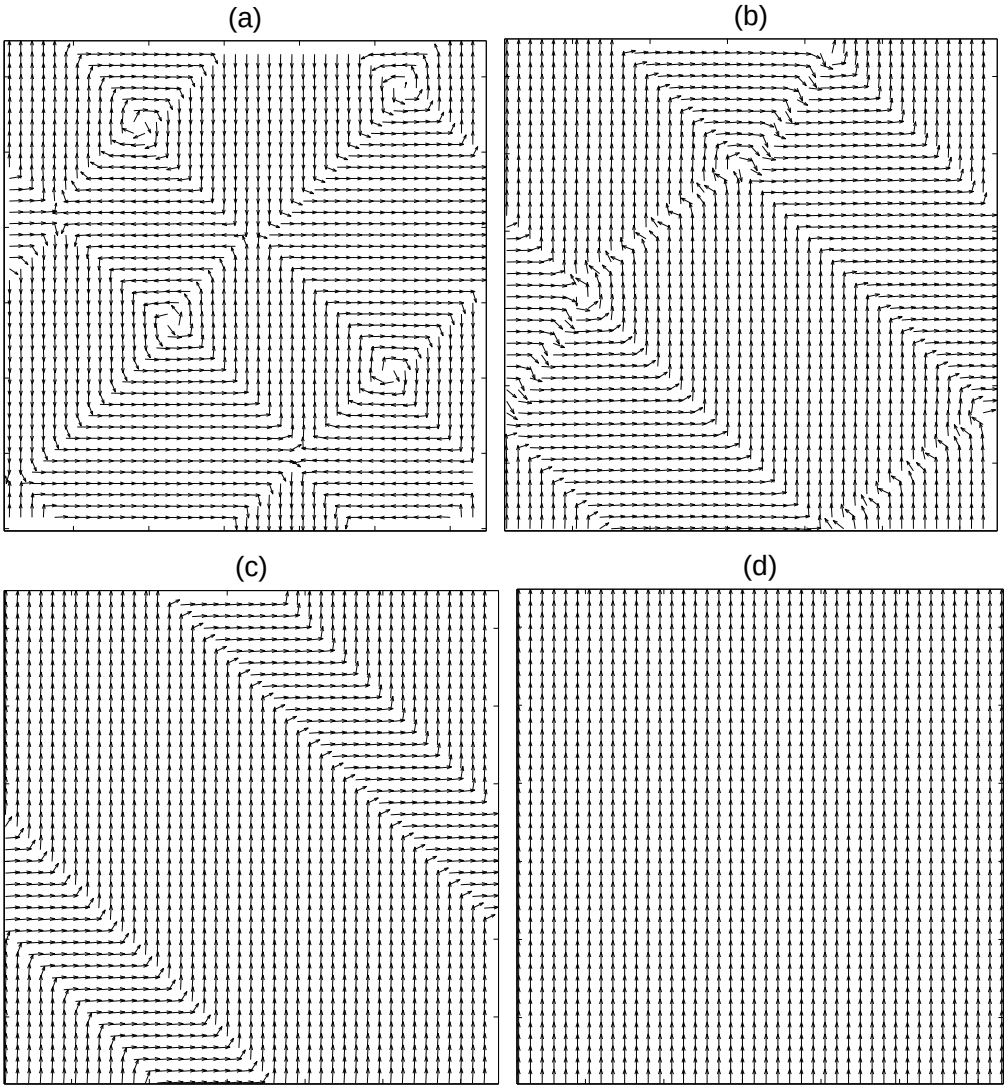

FIG. 1: Evolution of ferroelectric domains for a simulated (~ 0.85 μm $\times 0.85$ μ m) system at $T = 298K$. The electric field values are $E_x = 0, E_y = 0$ (snapshot (a)); $E_x = 0, E_y = 5.54$ kV/cm (snapshot (b)); $E_x = 0, E_y = 7.39$ kV/cm (snapshot (c)); $E_x = 0, E_y = 9.24$ kV/cm (snapshot (d));

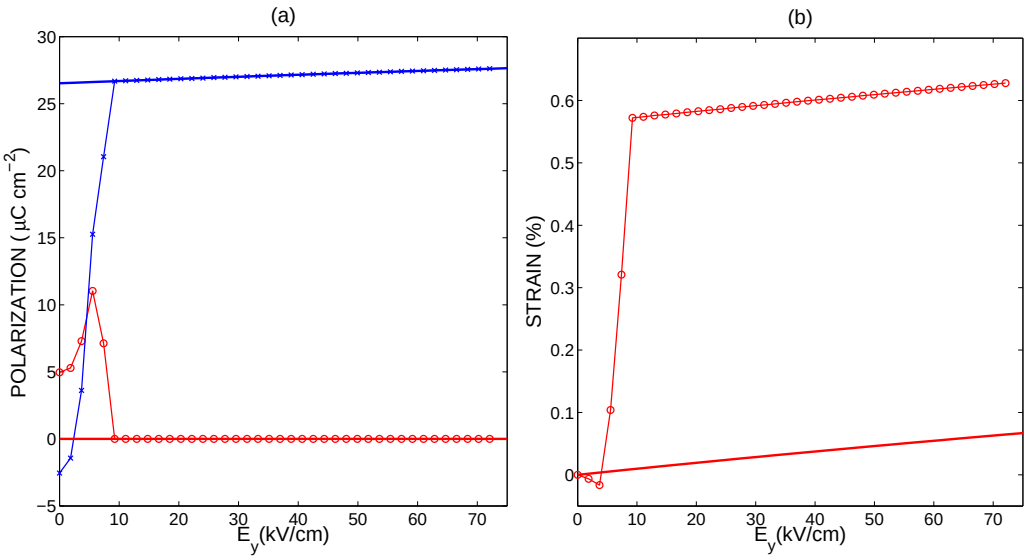

FIG. 2: (a) Variation of $\langle P_x \rangle$ (red line with circles) and $\langle P_y \rangle$ (blue line with crosses) with the applied field E_y for the evolution shown in Fig. 1. Also shown is the variation of P_x (red solid line) and P_y (blue solid line) obtained by minimizing only the free energy F_l ($\lambda = \mu = 0$), corresponding to a single domain state. (b) Variation of the uniaxial strain $\langle \eta_{yy}(E_y) \rangle - \langle \eta_{yy}(0) \rangle$ (red line with circles) with the electric field E_y. The corresponding single domain response is also shown (solid red line).

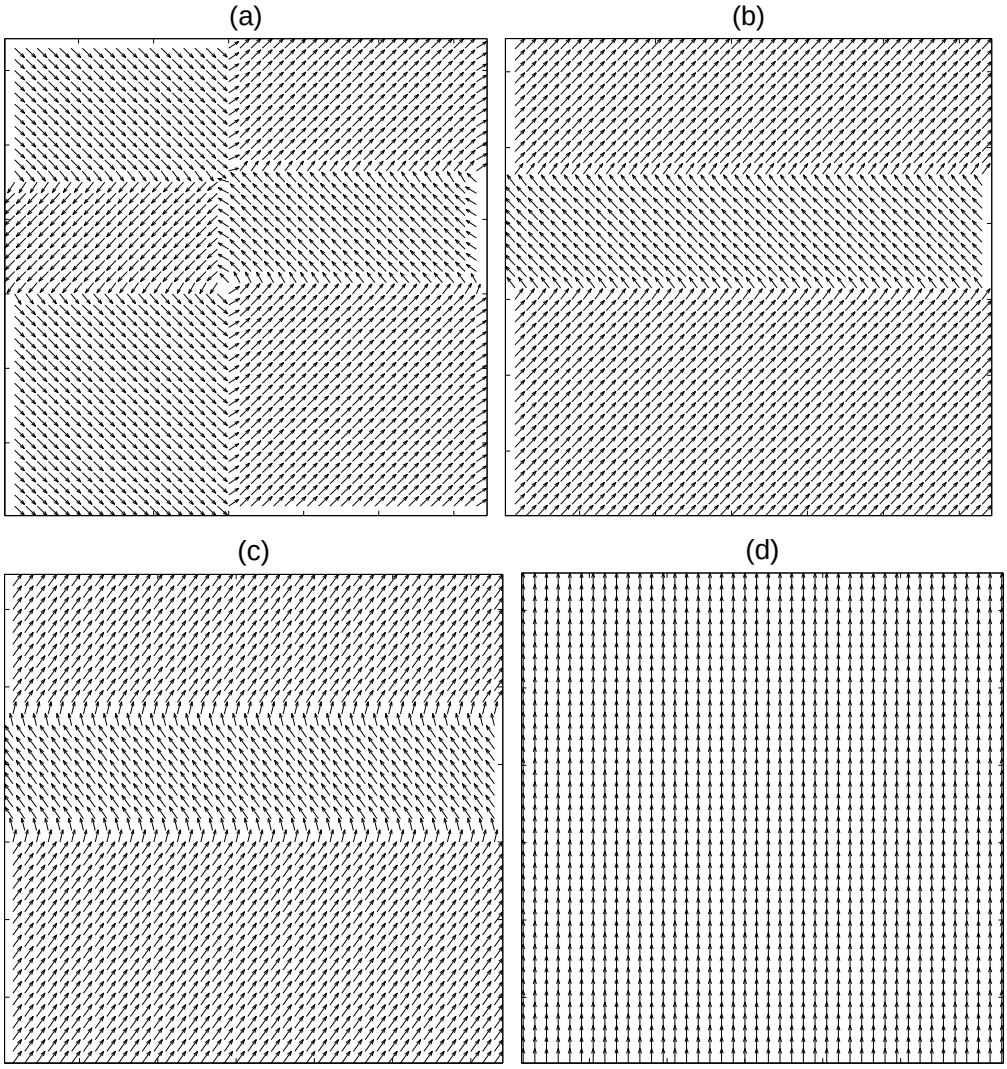

FIG. 3: Analogous to Fig. 1 but for $T = 273K$. The electric field values are $E_x = 0, E_y = 0$ (snapshot (a)); $E_x = 0, E_y = 5.54$ kV/cm (snapshot (b)); $E_x = 0, E_y = 51.74$ kV/cm (snapshot (c)); $E_x = 0, E_y = 53.59$ kV/cm (snapshot (d));

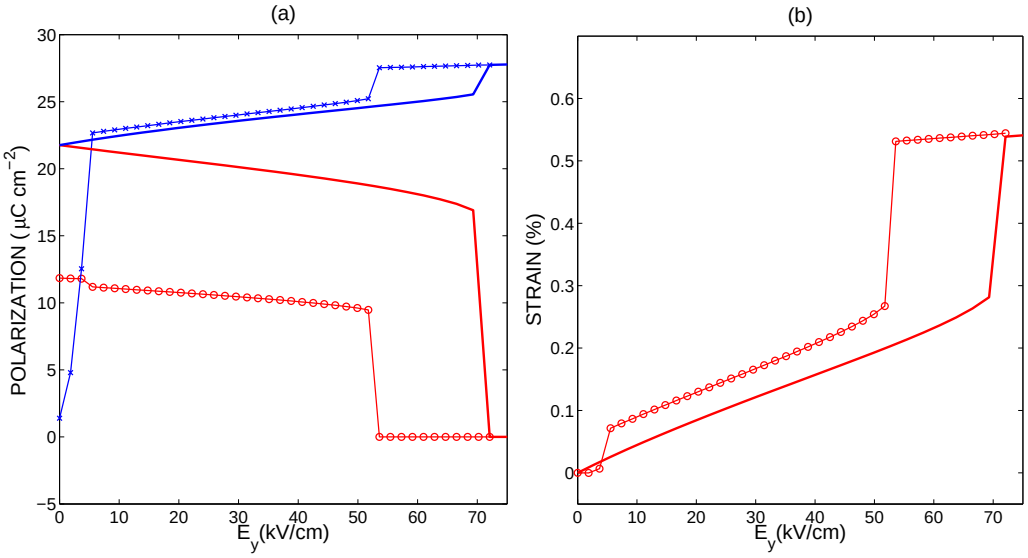

FIG. 4: (a) Variation of $\langle P_x \rangle$ (red line with circles) and $\langle P_y \rangle$ (blue line with crosses) with the applied field E_y for the evolution shown in Fig. 3. Also shown is the variation of P_x (red solid line) and P_y (blue solid line) for a single domain. (b) Variation of the uniaxial strain $\langle \eta_{yy}(E_y) \rangle - \langle \eta_{yy}(0) \rangle$ (red line with circles) with the electric field E_y. The corresponding single domain response is also shown (solid red line).